



ELSEVIER

journal homepage: www.intl.elsevierhealth.com/journals/cmpb

Detecting left ventricular impaired relaxation in cardiac MRI using moving mesh correspondences

Kumaradevan Punithakumar^{a,b,*}, Ismail Ben Ayed^c, Mariam Afshin^d,
Aashish Goela^e, Ali Islam^f, Shuo Li^g, Pierre Boulanger^{a,b,h}, Harald Becherⁱ,
Michelle Noga^{a,b}

^a Servier Virtual Cardiac Centre, Mazankowski Alberta Heart Institute, Edmonton, Alberta, Canada

^b Department of Radiology & Diagnostic Imaging, University of Alberta, Edmonton, Alberta, Canada

^c Ecole de Technologie Supérieure (ETS), University of Quebec, Montreal, QC, Canada

^d Dept. of Medical Imaging, Sunnybrook Health Science Centre, Toronto, ON, Canada

^e London Health Sciences Centre, London, ON, Canada

^f St. Joseph's Health Care, London, ON, Canada

^g Department of Medical Imaging and Medical Biophysics, University of Western Ontario, London, ON, Canada

^h Department of Computing Science, University of Alberta, Edmonton, Alberta, Canada

ⁱ Division of Cardiology, Department of Medicine, University of Alberta, Edmonton, Canada

ARTICLE INFO

Article history:

Received 3 May 2015

Received in revised form

21 September 2015

Accepted 20 October 2015

Keywords:

Cardiac left ventricle

Diastolic function

Image registration

Image segmentation

Magnetic resonance imaging

ABSTRACT

Anatomical cine cardiovascular magnetic resonance (CMR) imaging is widely used to assess the systolic cardiac function because of its high soft tissue contrast. Assessment of diastolic LV function has not regularly been performed due the complex and time consuming procedures. This study presents a semi-automated assessment of the left ventricular (LV) diastolic function using anatomical short-axis cine CMR images. The proposed method is based on three main steps: (1) non-rigid registration, which yields a sequence of endocardial boundary points over the cardiac cycle based on a user-provided contour on the first frame; (2) LV volume and filling rate computations over the cardiac cycle; and (3) automated detection of the peak values of early (E) and late ventricular (A) filling waves. In 47 patients cine CMR imaging and Doppler-echocardiographic imaging were performed. CMR measurements of peak values of the E and A waves as well as the deceleration time were compared with the corresponding values obtained in Doppler-Echocardiography. For the E/A ratio the proposed algorithm for CMR yielded a Cohen's kappa measure of 0.70 and a Gwet's AC1 coefficient of 0.70. Conclusion: Semi-automated assessment of the left ventricular (LV) diastolic function using anatomical short-axis cine CMR images provides mitral inflow measurements comparable to Doppler-Echocardiography.

© 2015 Elsevier Ireland Ltd. All rights reserved.

* Corresponding author at: Department of Radiology & Diagnostic Imaging, University of Alberta, Edmonton, Alberta, Canada.
Tel.: +1 780 407 1871.

E-mail address: punithak@ualberta.ca (K. Punithakumar).

<http://dx.doi.org/10.1016/j.cmpb.2015.10.015>

0169-2607/© 2015 Elsevier Ireland Ltd. All rights reserved.

1. Introduction

Most of the existing left ventricle (LV) assessment algorithms using cine cardiac magnetic resonance (CMR) focus on the systolic function, and are often limited to the analysis of regional wall motion abnormalities or the estimation of the ejection fraction [1–3]. However, the diastolic function is essential in the evaluation of various heart diseases, and several studies suggested that the assessment of the diastolic function is also important [4–7]. Heart failure with a preserved left ventricular ejection fraction represents approximately 40–50% of all cases of heart failure [7,8], and is increasing in prevalence among the senior population [9]. Furthermore, a distinction between systolic and diastolic heart failure is essential, given the importance of the therapeutic and prognostic differences between these two subsets of heart failures [10]. Therefore, early and accurate diagnosis of abnormalities in diastolic filling is of the utmost importance.

Although direct measurement of the LV filling pressures is preferable, the use of angiography is not ideal for routine clinical assessments as several non-invasive methodologies have become widely available [11]. Currently, 2D echocardiography using flow Doppler imaging is widely used to measure transmitral velocities. The existing echocardiography studies are based on Doppler measurements at the tips of the mitral valve leaflets to determine peak velocities of mitral inflow [9], Doppler echocardiography to estimate the mitral flow and pulmonary venous flow [12,13], and a color M-mode Doppler to estimate information such as the ventricular relaxation or compliance from transmitral velocity profile, among others. Despite these advances, transthoracic echocardiography (TTE) has important disadvantages, including a limited field of view due to the acoustic window, dependence on sample volume location, cosine θ errors relative to the flow direction, and the inability to image approximately 15–20% of the patients [5,11].

Although multiphase computed tomography (CT) can also be used for the analysis of the LV function, only a few studies were devoted to the analysis of the diastolic function. Boogers et al. presented a comparison between CT and 2D echocardiography using tissue Doppler imaging, noting good correlations for transmitral velocity, mitral septal tissue velocity, and estimation of the LV filling pressures [14].

Alternatively, CMR imaging allows for an exhaustive myocardial evaluation with high spatial resolution, and has several important advantages. They relax the need for geometric assumptions and afford an excellent image quality. Some CMR studies relied on phase contrast for the evaluation of the diastolic function [15–18,11]. In another study, a finite element based technique is used to estimate the diastolic dysfunction using tagged CMR images [19]. However, these CMR acquisition protocols are not commonly used in routine clinical practices due to their complex and time-consuming post processing and interpretation. Among other magnetic resonance sequences, anatomical cine CMR remains the most widely used sequence to assess the cardiac function [20]. Few notable exceptions that used the anatomical cine MR to assess the diastolic function include Wu et al. [21] who used long-axis views to compute mitral annulus sweep volume, and Mendoza et al. [22] who used short-axis view to compute LV volumes

and filling rates. Analysis of the diastolic function using short-axis view of the anatomical cine CMR requires delineation of LV from hundreds of images,¹ making manual segmentation impractical for standard clinical applications. Therefore, automated segmentation is important for the assessment of the diastolic function [23].

This study proposes a new method to assess the LV impaired relaxation using short-axis cine CMR images. The proposed method consists of a semi-automated LV segmentation approach and an automated detection of peak values of early and late ventricular filling waves. Given a user-provided segmentation of a single frame in a cardiac sequence, the proposed segmentation approach delineates endocardial borders of the LV via point-to-point correspondences. The moving mesh framework proposed in this study is fundamentally different from previous approaches [24,25]. Based on the concept of equivalent volume elements of a compact Riemannian manifold [26] and yielding a unique solution by solving a div-curl system, the proposed point-to-point approach prevents mesh folding, i.e., grid lines of the same grid family will not cross each other, an essential attribute in tracking cardiac tissues from a sequence of images.

2. Method

The proposed diastolic function analysis algorithm consists of preprocessing and detection of the E and A waves, the early and late (atrial) ventricular filling velocities, based on the computation of the LV filling rate curve. The proposed approach allows for evaluating the diastolic function for all the patients who undergo an CMR scan, including those who may not be primarily referred for a diastolic function evaluation. The method is based on three main steps: (1) non-rigid registration, which yields a sequence of points over time, given a user-provided contour on the first frame; (2) computations of the LV filling rate and volume over the cardiac cycle; and (3) automatic detections of the maxima of the E and A waves.

2.1. Preprocessing

Given a user-provided segmentation of a single frame in a cardiac sequence, the proposed method segments endocardial borders of the LV via point-to-point correspondences (refer to Fig. 1). We propose to use a moving mesh (or grid generation) framework [26] to compute point-to-point correspondences between the k th image T_k and $(k+1)$ th image T_{k+1} (for $k=1, \dots, K-1$) defined over $\Omega \subset \mathbb{R}^2$ (K is the total number of frames in a cardiac cycle), thereby obtaining a sequence of points over time (refer to Fig. 2). We state the problem as the optimization of a similarity/dissimilarity measure [27]:

$$\hat{\phi} = \arg \underset{\phi}{\text{opt}} E_s(T_k, T_{k+1}, \phi(\xi)) \quad (1)$$

where $\xi \in \Omega$ denotes pixel location, $\phi: \Omega \rightarrow \Omega$ a transformation function and $E_s(\cdot)$ a measure of similarity. As this problem may not have a unique solution, we introduce in the following a

¹ Typically 200 images per subject.

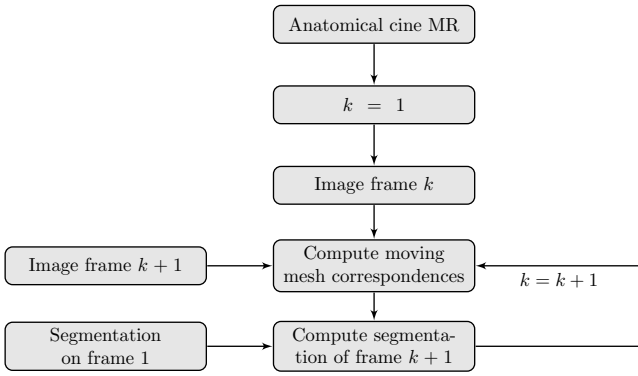


Fig. 1 – The proposed semi-automated delineation of the left ventricle.

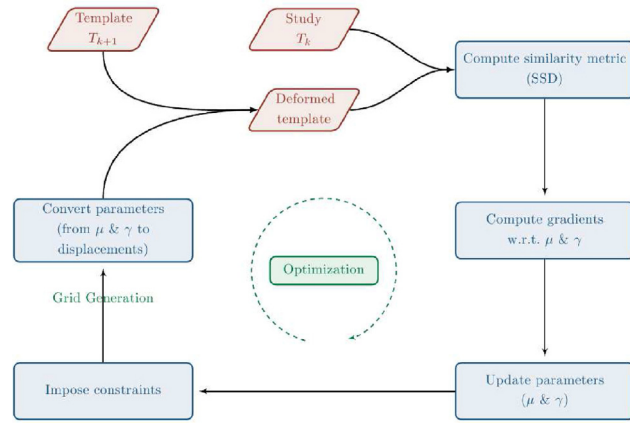


Fig. 2 – Computation of moving mesh correspondences.

deformation field using a monitor function μ and curl of end velocity field v , where $\mu : \Omega \rightarrow \mathbb{R}$ and $v : \Omega \rightarrow \mathbb{R}$.

2.1.1. Moving mesh generation

Let $\mu(\xi)$ be a continuous monitor function constrained by:

$$\int_{\Omega} \mu = |\Omega|. \tag{2}$$

The purpose of this step is to find a transformation $\phi : \Omega \rightarrow \Omega$, $\partial\Omega \rightarrow \partial\Omega$, so that

$$J_{\phi}(\xi) = \mu(\xi), \tag{3}$$

where J_{ϕ} denotes the Jacobian determinant of the transformation. The following computations yield a transformation ϕ , which verifies (3).

Step 1: Compute a vector field $\rho(\xi)$, which verifies

$$\text{div } \rho(\xi) = \mu(\xi) - 1. \tag{4}$$

Step 2: Build a velocity vector field from $\rho(\xi)$:

$$v_t(\xi) = \frac{\rho(\xi)}{t + (1-t)\mu(\xi)}, \quad t \in [0, 1], \tag{5}$$

where t is an artificially introduced (algorithmic) time.

Step 3: Finally, ϕ is obtained by solving the following ODE:

$$\frac{d\psi(\xi, t)}{dt} = v_t(\psi(\xi, t)), \quad t \in [0, 1], \quad \psi(\xi, t=0) = \xi, \tag{6}$$

and setting ϕ equal to ψ evaluated at $t=1$: $\phi(\xi) = \psi(\xi, t=1)$.

We add an additional constraint on the curl of $\rho(\xi)$ to (4). Then, we solve the ensuing div-curl system under the Dirichlet boundary condition to obtain a unique solution, as the above problem may have multiple solutions, i.e.,

$$\begin{cases} \text{div } \rho(\xi) = \mu(\xi) - 1 & \text{(a)} \\ \text{curl } \rho(\xi) = v(\xi) & \text{(b)} \end{cases} \tag{7}$$

with null boundary condition $\rho(\xi) = 0 \forall \xi \in \partial\Omega$, where $v(\xi)$ is a continuous function over Ω . Hence, the transformation can be fully parametrized by $J_{\phi}(\xi)$ and $v(\xi)$. We ensure the uniqueness of the solution using the Dirichlet boundary condition [28]. The Dirichlet boundary conditions may cause the motion errors to be higher at the image boundaries, and therefore, we pad both images by zeros.

With the above parametrization, we reformulate (1) as the following constrained optimization problem:

Problem. Given two images T_k and T_{k+1} , defined over Ω , find a function pair $\{\mu(\xi), v(\xi)\}$ that optimizes cost (1) s.t.:

$$\begin{cases} \int_{\Omega} \mu(\xi) d\xi = |\Omega| & \text{(a)} \\ \tau_h > \mu(\xi) > \tau_l, \quad \xi \in \Omega' \subset \Omega & \text{(b)} \end{cases} \tag{8}$$

where $0 < \tau_l$ ensuring that $\phi_{\mu,v}$ is a diffeomorphism, and Ω' is a sub-region of image domain Ω .

Constraint (8a) ensures that the areas of the domain and co-domain are equal after transformation, and constraint (8b) limits the amount of compressibility, which is controlled by parameters τ_l and τ_h , within sub-region Ω' . Note that a diffeomorphism corresponds to a positive transformation Jacobian determinant, which is enforced explicitly via the monitor function [26].

The above problem can be solved by a *step-then-correct* optimization strategy. We compute a sequence of corresponding points on the endocardial border in all the frames of a cardiac sequence using transformation function $\hat{\phi}$, given the segmentation on the first frame.

2.2. Detection of E and A waves

In order to detect the E and A waves, we need to compute the LV filling rate. The computation of the LV filling rate measurements is based on several processing steps. First, the LV volumes $\{V_k\}$ were computed for all k in the cardiac cycle, where V_k denotes the LV volume at k th cardiac

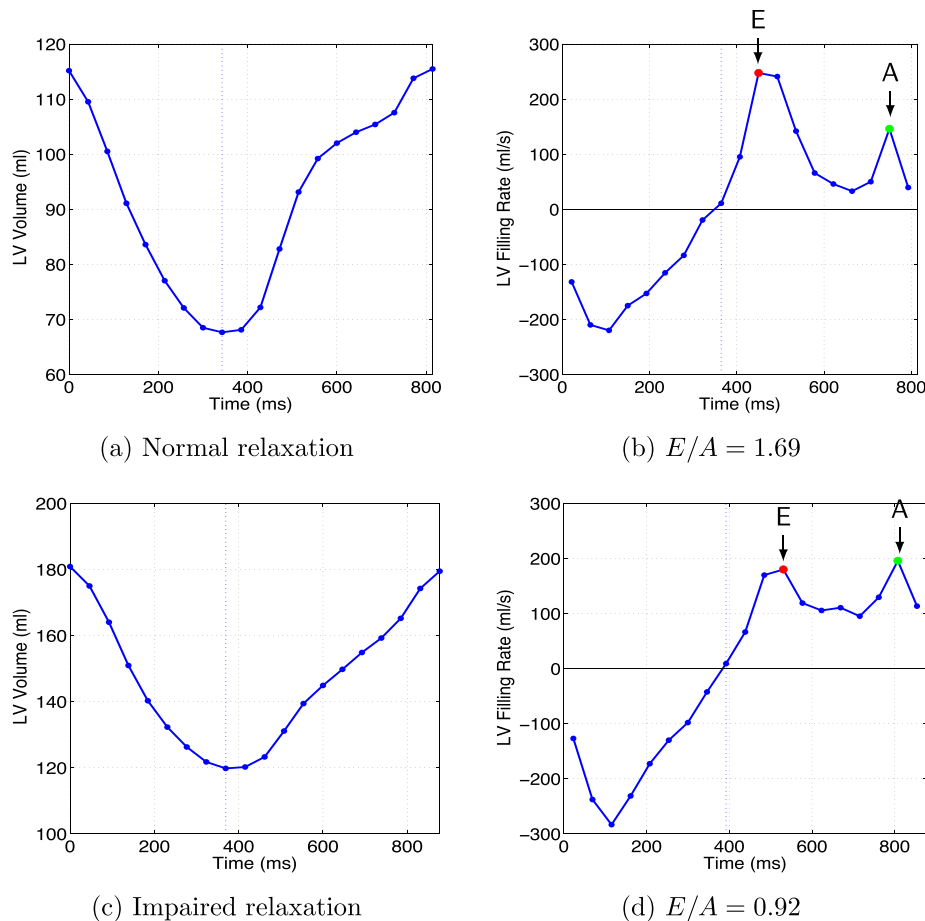


Fig. 3 – LV volume vs. time curves for: (a) typical normal relaxation; (b) typical impaired relaxation. Corresponding LV filling rate (dV_k/dt) curves are given by (c) and (d). The proposed method used LV volume curve to identify the start of the diastolic phase, and automatically detect the maximum values of E and A waves.

phase. For each cardiac phase, the contours for the LV cavities were automatically identified using the registration step above, given manual contours on the first frame. The papillary muscles were regarded as part of the LV cavity and were included in the LV volume computation. We used the short-axis image sequences that contain the LV cavity, and applied the Simpson's rule as well as the LV areas and slice spacing in computing volume V_k . This gives us V_k as a function of time step k (refer to Fig. 3(a) and (c)). We further compute the first derivative of the LV volumes with respect to time, thereby obtaining the LV filling rate dV_k/dt (refer to Fig. 3(b) and (d)).

E and A are the early and late (atrial) ventricular filling velocities, which can be computed using the LV filling rate. In normal subjects, the LV inflow velocity is at its highest point during early diastole (E wave), with a smaller LA contraction (A wave), which results in $E/A > 1$. In patients with impaired relaxation, the LV pressure rises at early diastole, which yields a decrease in the E wave. Furthermore, the left atrium contraction highly contributes to the LV filling, which yields an increase in the A wave. Therefore, the impaired relaxation yields $E/A < 1$.

In order to detect the peak values of the E and A waves, we first identify all the local maxima of the LV filling rate curve based on a first derivative test. Then, we select the highest and

second highest local maxima. The start of the diastolic phase is identified by detecting the time at which V_k is minimum. Among the two maxima, we take the one closer to the start of the diastolic phase as the E wave, and the other one as the A wave.

3. Results

Fifty-three patients (out of 100 patients collected retrospectively as a part of computer assisted image based cardiac disease diagnosis and monitoring study) who had undergone cardiac CMR and TTE with tissue Doppler imaging between 2007 and 2011 at London Health Sciences Centre University Hospital and St. Joseph's Hospital, London, Canada were included in the study. Inclusion criteria were: (1) the time difference between CMR and TTE exams is less than one year; and (2) TTE assessments included the peak early and late ventricular filling velocity values. Six patients were removed since the time differences between MR and TTE studies were more than one year. No patients were excluded based on CMR image quality or post-processing results. The mean and standard deviation of the time difference between the CMR and TTE exams for the 47 subjects included in the study is

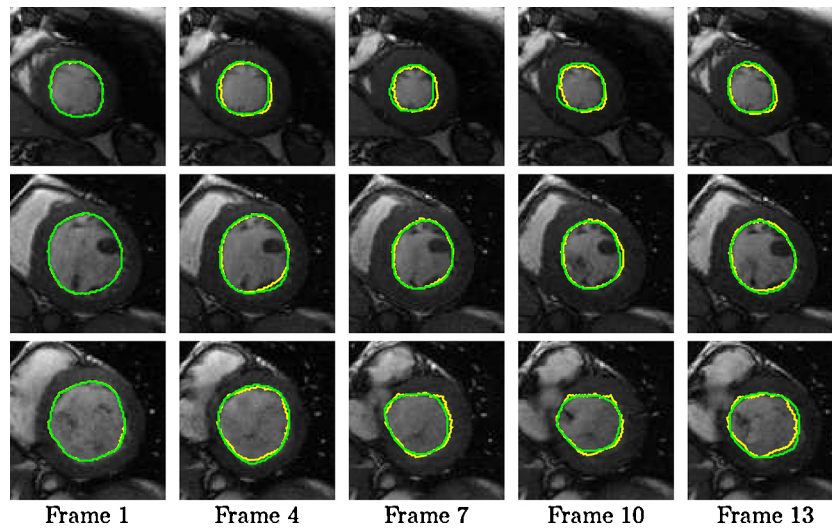


Fig. 4 – Representative examples of the LV boundary tracking using the proposed method (yellow) and the corresponding manual ground truth (green): apical (1st row), mid-cavity (2nd row) and basal (3rd row) frames. (For interpretation of the references to color in this figure legend, the reader is referred to the web version of this article.)

1.7 ± 2.6 months. All patients participating in this study had a clinical indication for cardiac MRI. The indications were coronary artery disease (13), valve disease (2), cardiomyopathy (7), myopericarditis (3), with the remainder of patients not having indications recorded. 9 patients were found to have global systolic dysfunction and 8 patients were found to have regional systolic abnormalities on MRI. There were no healthy volunteers.

The short-axis CMR image datasets consist of 20–25 functional 2D images per cardiac cycle. The CMR data were acquired on 1.5T CMR scanners with fast imaging employing steady state acquisition (FIESTA) mode. The data consists of images from 31 male and 16 female subjects, and the average age of subjects is 51.6 ± 16.7 years. The details of the datasets are presented in Table 1.

The size of the grid was selected automatically based on a bounding box containing the initial segmentation drawn on the first frame. A margin of 10 pixels around the bounding box was added to allow deformations outside the bounding box. For the step-then-correct algorithm, we set the threshold for the step-size to 0.01 and the maximum number of iterations to 25. The initial value of the step-size and the factor to reduce step-size were set to 0.5 and 2/3, respectively. Given the high variability in left ventricular motion, the following parameter

values were used for all cases so to allow large tissue deformations: $\tau_h = 4$ and $\tau_l = 0.1$.

In Fig. 4, we give a representative sample of the segmentation results (yellow) obtained using the proposed method and the corresponding ground truth manual contours (green) for apical, mid-cavity and basal frames.

Table 2 shows the parameters estimated using the proposed method. The parameters include ejection fraction (EF), end-diastolic volume (EDV), end-systolic volume (ESV) and stroke volume (SV). The table also reports mitral deceleration time which was computed using the LV filling rate for each subject.

Comparisons between the proposed method and TTE reports on diastolic function are given in Table 3. The following criteria was used for the classification: $E/A < 1$ corresponds to impaired relaxation; and $E/A \geq 1$ corresponds to normal, pseudonormal or Type 3 relaxation [5]. The proposed method and TTE findings agree that 18 and 22 subjects have impaired and normal/pseudonormal/Type 3 relaxations, respectively.

3.1. Cohen's kappa

We computed the Cohen's kappa coefficient [29] between the proposed method and TTE findings as follows.

$$\kappa = \frac{\Pr(a) - \Pr(e)}{1 - \Pr(e)} \quad (9)$$

Table 1 – Details of the datasets used in evaluation of the proposed method.

Description	Value
Number of patients	47
Patient age (mean ± std)	51.6 ± 16.7 years
Patient age range	16–79 years
Sex, m/f	31/16
Short-axis image size	(144 × 192)–(512 × 512) pixels
Number of frames (K)	20–25
Pixel spacing	(0.68 × 0.68)–(1.88 × 1.88) mm
Slice thickness	8–10 mm

Table 2 – Details of the global parameters computed using the proposed method.

Description	Value	Range
End-diastolic volume (ml)	121.4 ± 50.7	38.8–242.9
End-systolic volume (ml)	80.3 ± 47.1	18.1–205.3
Stroke volume (ml)	41.1 ± 14.9	20.6–83.5
Ejection fraction (%)	37 ± 13	13–61
Mitral deceleration time (ms)	141.1 ± 52.3	25.5–257.3

Table 3 – Detecting impaired relaxation in LV diastolic function using the proposed method and TTE. The following criteria was used for the classification: $E/A < 1$ corresponds to impaired relaxation; and $E/A \geq 1$ corresponds to normal, pseudonormal or Type 3 relaxation [5]. The bold values indicate the agreements between the methods (CMR and echo).

	TTE		Total
	Impaired relaxation	Normal, pseudonormal or Type 3 relaxation	
<i>Cine</i> CMR			
Impaired relaxation	18	1	19
Normal, pseudonormal, Type 3 relaxation	6	22	28
Total	24	23	47

The observed percentage agreement $Pr(a)$ is given by

$$Pr(a) = \frac{A + D}{N} \quad (10)$$

where A , D and N denote the number of times both methods classify a subject into impaired relaxation, the number of times both methods classify a subject into normal relaxation, and total number of subjects, respectively. The overall probability of random agreement $Pr(e)$ is given by

$$Pr(e) = \left(\frac{A1}{N} \times \frac{B1}{N} \right) + \left(\frac{A2}{N} \times \frac{B2}{N} \right) \quad (11)$$

where $A1 = A + C$, $A2 = B + D$, $B1 = A + B$, and $B2 = C + D$. B denotes the number of subjects classified into normal relaxation by CMR and impaired relaxation by TTE, and C vice versa.

The proposed method and TTE findings yielded a Cohen's Kappa coefficient of 0.70, a substantial agreement [30].

3.2. Gwet's AC1

Gwet's AC1 is computed by [31]:

$$AC1 = \frac{Pr(a) - e(\gamma)}{1 - e(\gamma)} \quad (12)$$

where

$$e(\gamma) = 2P_1(1 - P_1) \quad (13)$$

The approximate chance that a method (TTE or CMR) classifies a subject into impaired relaxation P_1 is given by

$$P_1 = \frac{A1 + B1}{2N} \quad (14)$$

The proposed method and TTE findings yielded a Gwet's AC1 coefficient of 0.70.

3.3. Reproducibility

Inter-observer and intra-observer variabilities were measured over a data set of 10 subjects. Two independent readers, blinded to TTE and each other's contours, traced the manual endocardial contours on the first frame. Intra-observer variability was evaluated based on one of the readers. Table 4 reports the inter-observer and intra-observer variabilities in terms of Intra Class Correlation (ICC), Bland-Altman test, and Pearson correlation coefficient (R). The parameters estimated using the proposed approach demonstrated good consistency in terms of ICC and Pearson correlation coefficient.

4. Discussion

This study demonstrated the utility of obtaining information about diastolic function from cine CMR sequences. An important advantage of our semi-automated method is that it significantly reduces the amount of time required for segmenting the left ventricle. This allows the user to analyse the function over the entire cardiac cycle in addition to the computation of common clinical measures such as ejection fraction or stroke volume. Our algorithm has the following advantages over prior LV segmentation works: (1) it removes the need for a time-consuming, manually-built training set; (2) it does not make prior assumptions as to the distributions of intensity and shape.

The proposed method relied on short-axis MR images to analyse the diastolic function which differs from the method by Wu et al. using two-, three-, and four-chamber views of the cine MR sequences [21]. The method by Wu et al. relied on the mitral annulus sweep volume to analyse the diastolic function and used only six points to estimate the mitral annulus using spline interpolation, whereas the proposed method relied on multiple points (around 30 points per segmentation) from about 10 short-axis slices to estimate the volume of the LV. Further, the method by Wu et al. required manual correction of atrioventricular junction tracking of about 30% of

Table 4 – Reproducibility of CMR diastolic function measurements.

	Intra-observer (cases = 10)			Inter-observer (cases = 10)		
	ICC (95% CI)	Bias (limits of agreement)	R	ICC (95% CI)	Bias (limits of agreement)	R
E (l/s)	1.00 (1.00, 1.00)	0.00 (−0.08, 0.08)	1.00	1.00 (0.99, 1.00)	0.019 (−0.470, 0.508)	0.99
A (l/s)	1.00 (1.00, 1.00)	0.02 (−0.06, 0.11)	1.00	0.97 (0.89, 0.99)	0.635 (−0.480, 1.751)	0.98
E/A	1.00 (1.00, 1.00)	−0.01 (−0.05, 0.03)	1.00	0.96 (0.84, 0.99)	−0.24 (−0.73, 0.26)	0.99
MDT (ms)	0.84 (0.48, 0.96)	−16.6 (−90.5, 57.3)	0.89	0.83 (0.46, 0.96)	3.9 (−61.9, 69.7)	0.84

the cases whereas no manual correction was employed for the proposed method. However, one of the disadvantages of using only the short-axis is that it is hard to include the effects of shortening of the heart along the long-axis. We are planning to address this problem by the fusing the information from long-axis slices in the future.

In contrast to the automated methods in [22,23], the proposed segmentation approach does not rely on intensity threshold for image segmentation. A major drawback of threshold-based segmentation approaches is that they offer a limited framework for strong prior incorporation [32], and often require a manual correction of the segmentation results. For example, 52% of the study population in [23] required manual correction of the LV contours. Segmentation of the LV is acknowledged as a challenging problem, and therefore, incorporation of prior knowledge is essential to increase the robustness and accuracy. The proposed approach allows for the incorporation of a strong prior, a user defined contour of the LV on the first frame. The method has been shown to be robust, and yielded accurate segmentation results in comparison to manually drawn contours for both left and right ventricles under various heart conditions [3,27,33]. Further, the proposed method demonstrated good consistency in reproducing similar results for inter-observer and intra-observer experiments.

The proposed method relies on the LV volume curves to compute the LV filling rates, and the early and late fillings are expressed in millilitres per second. These measurements are different from the TTE findings which measure the velocity of the blood flow through the mitral valve in centimetres per second. The peak values of the early and late filling ratios for velocity and flow will be the same only if the size of the mitral valve does not change during the diastolic phase. As well, the proposed method ignores the effect of mitral valve regurgitation when computing the early and late filling rates.

Another important MR measurement that can be used for the diagnosis of diastolic dysfunction is the phase contrast velocity measurement at the mitral valve. However, our data set was acquired retrospectively from the standard clinical scans, and therefore, only a small number of subjects (8 out of 47) had a phase contrast velocity scan at the mitral valve. As a future study, we are planning to compare the proposed methods against the mitral valve flow measurements with a larger data set.

There is a considerable variation in the size of the images in our data set ranging from 144×192 to 512×512 . However, the proposed method does not use prior information related to the relative size or shape of the ventricle, and therefore, the method was able to perform well regardless of the image size.

The proposed moving mesh algorithm retains a point-to-point correspondence along the frames of the image sequences. Therefore, it is possible to analyze the regional diastolic function. However, there are no known reference standard is available to compare the results.

5. Limitations of the proposed study

One of the limitations of our method is that it requires manual contouring of one time frame for a given slice position.

Although more time-consuming than automated methods, the proposed method allows for greater accuracy throughout the remainder of the cardiac cycle.

The study analysed the CMR and TTE data retrospectively and none of the patients had both exams on the same day. Although the maximum time difference between MR and TTE exams was one year, it might have resulted in changes in cardiac function for some of the subjects. This could be one of the reasons for the difference in diastolic function estimated by the proposed method and TTE findings.

We considered TTE exams as the reference standard to assess the performance of the proposed method since invasive hemodynamic procedures are not used for standard clinical investigations. TTE exams remain the generally accepted non-invasive reference method for diastolic function assessment [21]. The study did not also have the follow-up data to assess the prognostic significance of the proposed method.

The algorithm was tested over a dataset of only 47 subjects. However, the proposed algorithm will allow testing over a larger data set since it only requires minimal user input.

The LV volumes are computed based on short-axis slices of the MRI with 8–10 mm slice thickness, which might have impacted the volumetric assessment. The proposed analysis based on short-axis images also ignores the descent of the mitral valve through the short-axis plane during systole and ascent during diastole. In the future, we are planning to address these problems by tracking the mitral valve over the cardiac cycle using long-axis cine MR sequences.

6. Conclusions

In this study, we proposed a semi-automated approach to obtain information about the diastolic function using anatomical cine cardiac magnetic resonance (CMR) imaging. Our method detects the peak values of the E and A waves using the LV filling rate contour, thereby classifying the diastolic function into two categories: normal/pseudonormal/Type 3 and impaired. We performed experimental evaluations over CMR data sets acquired from 47 subjects, including comparisons with independent reports for the same subjects from TTE. For E/A ratio based classification, the proposed method correlated well with TTE, and yielded a Cohen's kappa measure of 0.70 and a Gwet's AC1 coefficient of 0.70. The diastolic function parameters estimated using the proposed approach also demonstrated good consistency in terms of Intra Class Correlation (ICC), Bland–Altman test, and Pearson correlation coefficient.

Conflicts of interest

None declared.

Ethical approval

The study was approved by the University of Western Ontario Research Ethics Board.

Funding

Part of this work was supported by a grant from Servier Canada Inc.

REFERENCES

- [1] A. Suinesiaputra, A. Frangi, T. Kaandorp, H. Lamb, J. Bax, J. Reiber, B. Lelieveldt, Automated detection of regional wall motion abnormalities based on a statistical model applied to multislice short-axis cardiac MR images, *IEEE Trans. Med. Imaging* 28 (4) (2009) 595–607.
- [2] M. Afshin, I. Ben Ayed, K. Punithakumar, M. Law, A. Islam, A. Goela, T. Peters, S. Li, Regional assessment of cardiac left ventricular myocardial function via MRI statistical features, *IEEE Trans. Med. Imaging* 33 (2) (2014) 481–494.
- [3] K. Punithakumar, I. Ben Ayed, A. Islam, A. Goela, I.G. Ross, J. Chong, S. Li, Regional heart motion abnormality detection: an information theoretic approach, *Med. Image Anal.* 17 (3) (2013) 311–324.
- [4] R.S. Bhatia, J.V. Tu, D.S. Lee, P.C. Austin, J. Fang, A. Haouzi, Y. Gong, P.P. Liu, Outcome of heart failure with preserved ejection fraction in a population-based study, *New Engl. J. Med.* 355 (3) (2006) 260–269.
- [5] J. Caudron, J. Fares, F. Bauer, J.-N. Dacher, Evaluation of left ventricular diastolic function with cardiac MR imaging, *Radiographics* 31 (1) (2011) 239–259.
- [6] T. Kuznetsova, L. Herbots, Y. Jin, K. Stolarz-Skrzypek, J. Staessen, Systolic and diastolic left ventricular dysfunction: from risk factors to overt heart failure, *Expert Rev. Cardiovasc. Ther.* 8 (2010) 251–258.
- [7] M. Maeder, D. Kaye, Heart failure with normal left ventricular ejection fraction, *J. Am. Coll. Cardiol.* 53 (11) (2009) 905–918.
- [8] T.E. Owan, D.O. Hodge, R.M. Herges, S.J. Jacobsen, V.L. Roger, M.M. Redfield, Trends in prevalence and outcome of heart failure with preserved ejection fraction, *New Engl. J. Med.* 355 (3) (2006) 251–259.
- [9] A. Prasad, J.L. Hastings, S. Shibata, Z.B. Popovic, A. Arbab-Zadeh, P.S. Bhella, K. Okazaki, Q. Fu, M. Berk, D. Palmer, N.L. Greenberg, M.J. Garcia, J.D. Thomas, B.D. Levine, Characterization of static and dynamic left ventricular diastolic function in patients with heart failure with a preserved ejection fraction, *Circ. Heart Fail.* 3 (2010) 617–626.
- [10] R.S. Vasan, D. Levy, Defining diastolic heart failure: a call for standardized diagnostic criteria, *Circulation* 101 (2000) 2118–2121.
- [11] V.K. Rathi, M. Doyle, J. Yamrozik, R.B. Williams, K. Caruppanan, C. Truman, D. Vido, R.W. Biederman, Routine evaluation of left ventricular diastolic function by cardiovascular magnetic resonance: a practical approach, *J. Cardiovasc. Magn. Reson.* 10 (2008) 10–36.
- [12] C. Appleton, J. Jensen, L. Hatle, J. Oh, Doppler evaluation of left and right ventricular diastolic function: a technical guide for obtaining optimal flow velocity recordings, *J. Am. Soc. Echocardiogr.* 10 (1997) 271–292.
- [13] M.M. Redfield, S.J. Jacobsen, J.C. Burnett Jr., D.W. Mahoney, K.R. Bailey, R.J. Rodeheffer, Burden of systolic and diastolic ventricular dysfunction in the community, *J. Am. Med. Assoc. (JAMA)* 289 (2) (2003) 194–202.
- [14] M.J. Boogers, J.M. van Werkhoven, J.D. Schuijf, V. Delgado, H.M. El-Naggar, E. Boersma, G. Nucifora, R.J. van der Geest, B.P. Paelinck, L.J. Kroft, J.H. Reiber, A. de Roos, J.J. Bax, H.J. Lamb, Feasibility of diastolic function assessment with cardiac CT, *J. Am. Coll. Cardiol. Cardiovasc. Imaging* 4 (3) (2011) 246–256.
- [15] E. Bollache, A. Redheuil, S. Clément-Guinaudeau, C. Defrance, L. Perdrix, M. Ladouceur, M. Lefort, A. De Cesare, A. Herment, B. Diebold, E. Mousseaux, N. Kachenoura, Automated left ventricular diastolic function evaluation from phase-contrast cardiovascular magnetic resonance and comparison with Doppler echocardiography, *J. Cardiovasc. Magn. Reson. (BioMed Central)* 12 (2010) 63–73.
- [16] G. Fernández-Pérez, R. Duarte, M.C. de la Calle, J. Calatayud, J.S. González, Analysis of left ventricular diastolic function using magnetic resonance imaging, *Radiología (English Ed.)* 54 (4) (2012) 295–305.
- [17] B. Graca, M. Ferreira, P. Donato, M. Castelo-Branco, F. Caseiro-Alves, Cardiovascular magnetic resonance imaging assessment of diastolic dysfunction in a population without heart disease: a gender-based study, *Eur. Radiol.* 24 (1) (2014) 52–59.
- [18] J.J. Hartiala, G.H. Mostbeck, E. Foster, N. Fujita, M.C. Dulce, A.F. Chazouilleres, C.B. Higgins, Velocity-encoded cine MRI in the evaluation of left ventricular diastolic function: measurement of mitral valve and pulmonary vein flow velocities and flow volume across the mitral valve, *Am. Heart J.* 125 (4) (1993) 1054–1066.
- [19] V.Y. Wang, H. Lam, D.B. Ennis, B.R. Cowan, A.A. Young, M.P. Nash, Modelling passive diastolic mechanics with quantitative MRI of cardiac structure and function, *Med. Image Anal.* 13 (5) (2009) 773–784.
- [20] A. Bistoquet, J. Oshinski, O. Skrinjar, Left ventricular deformation recovery from cine MRI using an incompressible model, *IEEE Trans. Med. Imaging* 26 (9) (2007) 1136–1153.
- [21] V. Wu, J.Y. Chyou, S. Chung, S. Bhagavatula, L. Axel, Evaluation of diastolic function by three-dimensional volume tracking of the mitral annulus with cardiovascular magnetic resonance: comparison with tissue Doppler imaging, *J. Cardiovasc. Magn. Reson.* 16 (1) (2014) 71.
- [22] D.D. Mendoza, N. Codella, Y. Wang, M.R. Prince, S. Sethi, S.J. Manoushagian, K. Kawaji, J.K. Min, T.M. LaBounty, R.B. Devereux, et al., Impact of diastolic dysfunction severity on global left ventricular volumetric filling-assessment by automated segmentation of routine cine cardiovascular magnetic resonance, *J. Cardiovasc. Magn. Reson.* 12 (2010) 46.
- [23] K. Kawaji, N.C. Codella, M.R. Prince, C.W. Chu, A. Shakoor, T.M. LaBounty, J.K. Min, R.V. Swaminathan, R.B. Devereux, Y. Wang, J.W. Weinsaft, Automated segmentation of routine clinical cardiac magnetic resonance imaging for assessment of left ventricular diastolic dysfunction, *Circ. Cardiovasc. Imaging* 2 (6) (2009) 476–484.
- [24] B. Li, Y. Liu, C. Occlshaw, B. Cowan, A. Young, In-line automated tracking for ventricular function with magnetic resonance imaging, *J. Am. Coll. Cardiol. Cardiovasc. Imaging* 3 (8) (2010) 860–866.
- [25] B. Li, A.A. Young, B.R. Cowan, GPU accelerated non-rigid registration for the evaluation of cardiac function, in: D. Metaxas, et al. (Eds.), in: *Medical Image Computing and Computer-Assisted Intervention (MICCAI)*, vol. 5242, Springer, Berlin, Heidelberg, 2008, pp. 880–887.
- [26] J. Liu, New development of the deformation method (Ph.D. thesis), Department of Mathematics, The University of Texas at Arlington, 2006.
- [27] H.-M. Chen, A. Goela, G.J. Garvin, S. Li, A parameterization of deformation fields for diffeomorphic image registration and its application to myocardial delineation, in: *Medical Image Computing and Computer Assisted Intervention*, vol. 6361, 2010, pp. 340–348.
- [28] X. Zhou, On uniqueness theorem of a vector function, *Prog. Electromagn. Res.* 65 (2006) 93–102.

- [29] J. Cohen, A coefficient of agreement for nominal scales, *Educ. Psychol. Meas.* 20 (1) (1960) 37–46.
- [30] A.J. Viera, J.M. Garret, Understanding interobserver agreement: the kappa statistic, *Family Med.* 37 (5) (2005) 360–363.
- [31] K.L. Gwet, *Handbook of Inter-rater Reliability: The Definitive Guide to Measuring the Extent of Agreement Among Multiple Raters*, 3rd ed., Advanced Analytics, LLC, Gaithersburg, MD, USA, 2012.
- [32] C. Petitjean, J.-N. Dacher, A review of segmentation methods in short axis cardiac MR images, *Med. Image Anal.* 15 (2) (2011) 169–184.
- [33] K. Punithakumar, M. Noga, I. Ben Ayed, P. Boulanger, Right ventricular segmentation in cardiac MRI with moving mesh correspondences, *Comput. Med. Imaging Gr.* 43 (2015) 15–25.